Osteoarthritis and Cartilage 27 (2019) 1711–1720

Osteoarthritis and Cartilage

Human articular cartilage mechanosensitivity is related to histological degeneration – a functional MRI study

S. Nebelung † *, M. Post †, M. Knobe ‡, D. Shah †, C. Schleich §, L. Hitpass †, C. Kuhl †, J. Thüring †, D. Truhn † ||

† *Department of Diagnostic and Interventional Radiology, Aachen University Hospital, Aachen, Germany*
‡ *Department of Orthopaedic Trauma, Aachen University Hospital, Aachen, Germany*
§ *Department of Diagnostic and Interventional Radiology, University of Düsseldorf, Düsseldorf, Germany*
|| *Institute of Imaging and Computer Vision, RWTH Aachen University, Aachen, Germany*

ARTICLE INFO

Article history:
Received 15 February 2019
Accepted 3 July 2019

Keywords:
T1ρ
Cartilage
MRI
Loading
Tissue functionality

SUMMARY

Objective: To investigate changes in response to sequential pressure-controlled loading and unloading in human articular cartilage of variable histological degeneration using serial T1ρ mapping.
Method: We obtained 42 cartilage samples of variable degeneration from the medial femoral condyles of 42 patients undergoing total knee replacement. Samples were placed in a standardized artificial knee joint within an MRI-compatible whole knee-joint compressive loading device and imaged before (δ_0), during (δ_{ld1}, δ_{ld2}, δ_{ld3}, δ_{ld4}, δ_{ld5}) and after (δ_{rl1}, δ_{rl2}, δ_{rl3}, δ_{rl4}, δ_{rl5}) pressure-controlled loading to 0.663 ± 0.021 kN (94% body weight) using serial T1ρ mapping (spin-lock multigradient echo sequence; 3.0T MRI system [Achieva, Philips]). Reference assessment included histology (Mankin scoring) and conventional biomechanics (Tangent stiffness). We dichotomized sample into *intact* ($n = 21$) and *degenerative* ($n = 21$) based on histology and analyzed data using Mann Whitney, Kruskal Wallis, one-way ANOVA tests and Spearman's correlation, respectively.
Results: At δ_0, we found no significant differences between intact and degenerative samples, while the response-to-loading patterns were distinctly different. In intact samples, T1ρ increases were consistent and non-significant, while in degenerative samples, T1ρ increases were significantly higher ($P = 0.004$, δ0 vs δld1, δ0 vs δld3), yet undulating and variable. With unloading, T1ρ increases subsided, yet were persistently elevated beyond δ0.
Conclusion: Cartilage mechanosensitivity is related to histological degeneration and assessable by serial T1ρ mapping. Unloaded, T1ρ characteristics are not significantly different in intact vs degenerative cartilage, while load bearing is organized in intact cartilage and disorganized in degenerative cartilage.

Introduction

Articular cartilage is an exquisitely mechanosensitive tissue and its structure and composition are defined by the mechanical environment[1]. Cartilage degeneration, i.e., the hallmark change of osteoarthritis (OA), is considered the consequence of abnormal tissue remodelling processes driven by inflammation, unfavourable biomechanical conditions and predisposing tissue susceptibility[2]. Physiological loading of cartilage is chondroprotective and decreases the incidence of OA, while unphysiological loading is detrimental to homeostasis and integrity[3]. By combining mechanical loading and advanced Magnetic Resonance Imaging (MRI) techniques, we can further define cartilage functionality non-invasively. As softening is a decisive change in early cartilage degeneration[4], studying tissue functionality constitutes a promising surrogate parameter to identify early, potentially reversible stages of degeneration[5–8]. Researchers have applied a myriad of quantitative MRI parameters to assess articular cartilage composition beyond structure[9,10]. T1ρ is promising as it provides a

* Address correspondence and reprint requests to: S. Nebelung, Department of Diagnostic and Interventional Radiology Aachen University Hospital Pauwelsstrasse 30 52074 Aachen, Germany. Tel: 49-241-80-36165; Fax: 49-241-80-82453.
E-mail addresses: snebelung@ukaachen.de (S. Nebelung), manuel.post@rwth-aachen.de (M. Post), mknobe@ukaachen.de (M. Knobe), dshah@ukaachen.de (D. Shah), Christoph.Schleich@med.uni-duesseldorf.de (C. Schleich), lhitpass@ukaachen.de (L. Hitpass), ckuhl@ukaachen.de (C. Kuhl), jthuering@ukaachen.de (J. Thüring), dtruhn@ukaachen.de (D. Truhn).

https://doi.org/10.1016/j.joca.2019.07.006
1063-4584/

quantitative measure of macromolecular content and biologically relevant changes. However, its exact structural and/or compositional determinants are still debated and specificity to distinct cartilage constituents is limited[11,12]. Furthermore, reports on loading-induced changes in T1ρ are inconsistent. Souza *et al.* found significant decreases in T1ρ in the tibial cartilage only, while changes in femoral cartilage were discrepant[5,7]. Hamada *et al.* reported decreases in T1ρ[13], while our group found consistent increases[8,14]. Although these studies differed in design, loading protocol, tissue source and reference standard, cartilage functionality has been related to tissue degeneration. To this end, a standardized setup was implemented to functionally assess cartilage samples of variable histological degeneration *in situ*. Our study's hypothesis was that loading induces distinctly different changes in T1ρ in intact as opposed to degenerative cartilage, and that these changes are related to the tissue's altered biomechanical properties.

Materials and methods

Industry support

Philips Healthcare (Hamburg, Germany) supported this study by providing the T1ρ sequence. The authors had and have full control over the data and information submitted for publication.

Study design

We designed this study as a prospective *ex-vivo* imaging study of human cartilage. Prior to the study, we obtained local Institutional Review Board approval (Ethical Committee, RWTH Aachen University, Germany, AZ-EK157/13) and individual written informed patient consent.

Cartilage sample preparation

As in previous studies[8,14–16], we obtained cartilage-bone material from 42 patients undergoing total knee replacement at our institution (13 men, 29 women; mean age, 73.2 years [range, 61–87 years]). The inclusion criterion was primary osteoarthritis of the knee as determined radiographically (i.e., Kellgren–Lawrence grades $\geq$2[17]), while exclusion criteria were all forms of secondary OA, a positive history of previous trauma and/or surgery and other bone and joint disorders.

After excision, we collected the cartilage-bone material in sterile Dulbecco's modified Eagle's medium (DMEM) with 100 U/ml penicillin, 100 μg/ml gentamycin and 1.25 U/ml amphotericin-B (Gibco-BRL, Gaithersburg, US) and prepared it according to standard. First, we identified the medial femoral condyle and harvested samples from its central weight-bearing region for the sake of topoanatomic consistency, i.e., to obtain samples of similar geometry[18]. Second, we prepared cylindrical osteochondral samples using an 8 mm-diameter skin biopsy punch (pfm-medical, Cologne, Germany) and cut these samples to standard height of 3 mm using a custom-made metal block with circular molds (3 mm deep). We took care to cut the cartilage-bone material directly above the subchondral lamella and in a non-tilted position to obtain a horizontal cutting plane. Third, we confirmed sample height of 3 mm using a standard digital micrometer (Mitutoyo 293–521, Tokyo, Japan). Finally, in keeping with this study's premise of differentiating response-to-loading patterns as a function of degeneration, we only included normal, slightly and moderately degenerative samples (i.e., ICRS grades 0, 1 and 2[19]) upon macroscopic evaluation by the first author (SN). Consequently, we excluded more severely degenerative samples. Additionally, we prepared macroscopically grossly similar tissue regions (as the chondral sample) from adjacent cartilage-bone areas and sectioned these parallel to the mid-coronal plane to allow for the histological evaluation of the osteochondral junction.

We estimated a minimum sample size of 27 based on an earlier study[16] and a dedicated online tool (http://www.statstodo.com ["Sample sizes for two groups"]) (statistical power 0.9, type-I error 0.05, mean paired difference 5.1, standard deviation 5.7). To increase statistical power and alleviate the effects of post-hoc sample allocation based on histology, we prepared an extended number of 42 samples. One sample was harvested from each patient to avoid sample pooling.

Compressive loading device

In this study, we used a pressure-controlled MRI-compatible whole-knee joint compressive loading device for quasi-static uniaxial compressive loading of cartilage samples. This device is based on a previous version[15]. Briefly, we scanned a right human knee by CT and 3D-printed femoral and tibial bone models of the standardized knee joint that were covered by cartilage-mimicking polyvinyl-siloxane (wirosil®, Bego, Bremen, Germany). Native cartilage samples (see **2.3 Cartilage sample preparation**) were placed into a standard defect (8 mm diameter, 3 mm depth) at the central medial femoral condyle. Substantial stress relaxation (of up to 48% after 45min) and non-uniformity of intra-tissue strains[15,20], however, necessitated modifications to improve standardisation and reproducibility. To this end, we integrated a custom-made pneumatic actuation mechanism on the mobile tibial side and connected it to standard hospital pressure lines providing a maximum pressure of 4.69 bar (open-valve position). Pressure levels were digitally regulated by an electrically actuated valve (Festo, Esslingen, Germany) and control of customized software routines (LabView, National Instruments Corporation, Austin, US). By control of pressure, the mobile tibia was displaced towards the fixed femur to induce constant pressurization of the cartilage sample. Effective load at 4.69 bar target pressure was 0.663 ± 0.021 kN (whole joint) and 819.0 ± 11.4 kPa (cartilage sample). Longitudinal measurements over 45 min revealed no relevant loss in force (0.653 ± 0.005 kN). We directly attached a single-channel receive-only endorectal coil (BPX-30, Medrad-Bayer, Leverkusen, Germany) to the medial joint space to improve the signal-to-noise ratio at the medial compartment. Additional details are shown in Fig. 1 and appended as Supplementary Material.

MRI measurements and data analysis

Following placement of the native cartilage sample in the standardized knee joint, the thus loaded device was centrally positioned in a clinical 3.0T scanner (Achieva, Philips, Netherlands). We performed serial MRI measurements at three consecutive configurations, i.e., unloaded (δ_0), loaded (δ_{ld}) and unloaded (δ_{rl} [relaxed]). At δ_0, we acquired proton density-weighted (PDW) sequences in the coronal, sagittal and axial planes (Table I) to confirm proper sample position and guide the coronal section along the mid-coronal plane. The first (unloaded) T1ρ images were acquired along the mid-coronal plane for reference purposes (δ_0). Subsequently, we loaded the sample to 4.69 bar (i.e., open-valve position) to actuate loading to 0.663 ± 0.021 kN (i.e., 94% body weight [based on 70.8 kg mean adult body weight[21]). Concurrently, we initiated five serial T1ρ image acquisitions (δ_{ld1}, δ_{ld2}, …, δ_{ld5}) at constant loading conditions and without any prior equilibration. Once these measurements were completed, we released pressure to ambient levels and initiated five serial T1ρ image acquisitions instantaneously to assess sample relaxation (δ_{rl1}, δ_{rl2}, …, δ_{rl5}) (Fig. 2(a)). We

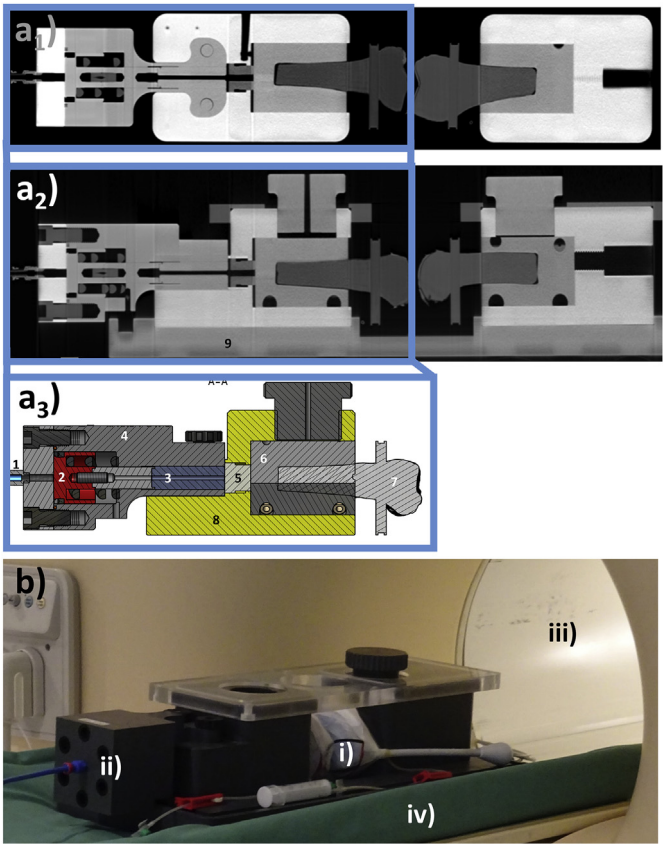

Fig. 1. Detailed representation of modified whole-knee joint loading device. Axial (a_1) and sagittal (a_2) cross-sectional CT views of the device and corresponding 2-D CAD scheme of the pneumatically driven actuation mechanism (a_3) (framed in blue). Pressure is supplied via pressure port (1) to actuate the pneumatic piston (2, red) which is connected to the piston shaft and its extension (3). The entire pneumatic mechanism is contained within a dedicated encasement (4) and the actuation force is translated via a specific adapter (5) and paired holding shells (6) to support the specific anatomical tibial bone model (7). The tibia-sided components are contained within a fixation mount (8) attached to the rigid base plate (9). Whole-knee joint loading device positioned on the patient bed within the MRI scanner (b). The endorectal coil (i) is positioned at the medial compartment and centred on the joint line. The joint capsule is filled with standard PBS buffer. Encased pneumatic (ii), bore of MRI scanner (iii) and patient bed (iv).

Table I
Acquisition Parameters of MRI sequences

	PDW	T1ρ
Sequence Type	Turbo spin echo	Spin-lock multi-gradient echo
Orientation	ax, sag, cor	cor
Repetition Time [ms]	4,057	30
Echo time [ms]	15	2.91
Turbo spin-echo factor	14	64
Field of view [mm]	110 × 110	30 × 30
Acquisition matrix	352 × 278	64 × 64
Reconstruction matrix	512 × 512	80 × 80
Resolution [mm/pixel]	0.21 × 0.21	0.38 × 0.38
Flip angle [°]	90	11
Number of signal averages	1	4
Slices	28	7
Slice Thickness [mm]	3.0	3.2
Interslice Gap [mm]	3.3	3.2
Spin-lock durations [ms]	n/a	0, 10, 20, 30, 40
Duration [min]	4.3	7.4

PDW – Proton Density-weighted, ax – axial, sag – sagittal, cor - coronal. n/a - not applicable.

confirmed stable sample positioning using the morphological T1ρ images. Measurements were performed at room temperature and monitored during one series (20.2 ± 0.3°C).

We performed data analysis as before[8] to generate spatially resolved quantitative T1ρ maps. To this end, we imported the MR raw data into Matlab R2017a software (Natick, MA, USA) and calculated T1ρ relaxation time constants for each pixel of the mid-coronal image using the following mono-exponential fitting routine:

$$\text{Signal (TSL)} = A \exp(-\text{TSL} / T1\rho) \quad (1)$$

Here, TSL is the duration of the spin-lock pulses, T1ρ the target relaxation time constant and A the signal pre-factor. We used R^2 statistics adjusted to the degrees of freedom to ascertain fit quality ($R^2 > 0.95$). DT segmented sample outlines manually based on the mid-coronal PDW image by choosing pixels that safely lay within the sample. By excluding boundary pixels, i.e., those pixels at the sample's surface that neither lay completely within nor outside the sample volume, partial volume effects were reduced. By visual inspection, SN and DT validated segmentation outlines against the morphological PDW (and processed T1ρ) images and the histological sections. To account for loading-induced loss in sample height, we adapted segmentation outlines using the last T1ρ image obtained during loading (i.e., δ_{ld5}), and we used this segmentation mask for segmentation of δ_{ld1} to δ_{ld4}. Similarly, to account for adaptive processes with relaxation, we used the first T1ρ image after unloading (i.e., δ_{rl1}) for segmentation outlines during relaxation. Mean sample heights and widths were determined based on these segmentation masks (i.e., δ_0, δ_{ld5}, δ_{rl1}). Repeatability of the segmentation process was not assessed. We performed further zonal analysis by automatically partitioning the sample outlines into two equal layers based on pixel-wise measurements of sample height. Thus, sample halves at the surface (superficial, sf) and towards the subchondral bone (deep, dp) were obtained. Regions-of-interest were the entire cartilage sample (ECS) and the superficial (sf) and deep (dp) layers that were defined individually for each sample, loading and relaxation position and measured in terms of pixel numbers. Due to the layer-wise approach, sf and dp layers had equal pixel numbers per segmentation outline.

Reference evaluation

Biomechanical analysis

After the MRI measurements, we retrieved the chondral sample. We used a Zwick/Roell Z2.5 universal mechanical testing machine (Ulm, Germany) equipped with a 20 mm-diameter compressive piston and a 200 N-load cell for biomechanical testing as before[8] and performed unconfined compression tests at 0.005%/s strain rate to 21% maximum strain while recording load–displacement data simultaneously using TestXpert software (Zwick/Roell). We chose a relatively low strain rate to evaluate the contribution of the extracellular matrix (ECM), which bears the majority of loading at a strain rate of 0.005%/s[22], and determined the tangent stiffness (TS) based on the stress–strain ratio by fitting a tangent to the strain range of 10–20%[23].

Histological analyses

Next, the chondral samples underwent standard histological work-up[8,16]. Samples were fixed in paraformaldehyde, sectioned along the mid-coronal plane, embedded in paraffin, cut to 5-μm sections, stained with hematoxylin/eosin and Safranin O and imaged using a standard light microscope (Leica DM/LM-P, Wetzlar,

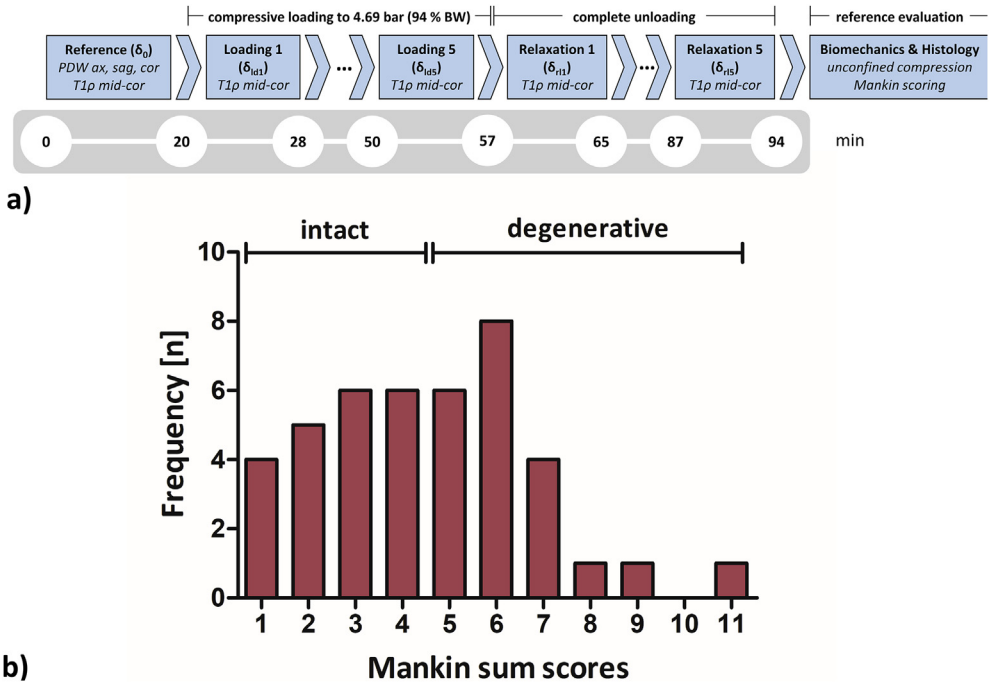

Fig. 2. a) Time schedule of serial T1ρ image acquisitions. Measurements under loading ($\delta_{ld1\text{-}5}$) and relaxation conditions ($\delta_{rl1\text{-}5}$) were performed serially without equilibration periods. PDW - proton density-weighted; ax - axial; sag - sagittal; cor - coronal; mid-cor - mid-coronal, δ_0 – unloaded reference configuration; min - minutes. b) Distribution of Mankin sum scores; $n = 21$ samples each constituted the intact and degenerative subgroups following sample dichotomization.

Germany). Following simultaneous decalcification and fixation in Ossa fixona (Diagonal, Münster, Germany), the adjacent osteochondral sections were prepared similarly.

Two experienced investigators (SN [experience in musculoskeletal histopathology] 8 years; MP [experience in musculoskeletal histopathology] 3 years) performed the semi-quantitative histological assessment of cartilage degeneration according to the Mankin classification[24] which assesses structural (score, 0–6), cellular (score, 0–3), proteoglycan staining-associated (score, 0–4) and tidemark integrity-associated (score, 0–1) tissue features. These features are summed up to give the Mankin sum score (MSS; range, 0–14) with higher scores indicating more severe degeneration. The investigators assessed histological sections individually and if scores were different, sections were discussed until consensus. Tidemark integrity was evaluated on adjacent osteochondral sections, while structure, cells and proteoglycan staining were assessed on the chondral samples. Samples were dichotomized as intact (*int*, MSS 0–4, Mankin grade 0) or degenerative (*deg*, MSS $\geq$ 5, Mankin grade $\geq$ I) based on the sample's MSS as before[25].

Statistical analyses

The first author (SN) performed the statistical analyses using GraphPad Prism (v6.0, San Diego, CA, US). In the following, δ_0 refers to the absolute T1ρ values in the unloaded configuration, while $\delta_{ld[x]}$ and $\delta_{rl[x]}$ refer to the absolute T1ρ values in the loaded ($\delta_{ld[x]}$) or relaxed configurations ($\delta_{rl[x]}$) at measurement x (of five serial measurements each). Relative changes in T1ρ are referred to as ΔT1ρ and were calculated by relating the absolute T1ρ values at $\delta_{ld1\text{-}5}$ (or $\delta_{rl1\text{-}5}$) to δ_0, respectively. For example, T1ρ at δ_{ld1} (connoted as $\Delta T1\rho(\delta_{ld1})$ was calculated as $\Delta T1\rho(\delta_{ld1})=((\delta_{ld1}/\delta_0)\text{-}1)*100)[\%]$. Following sample dichotomization into *int* and *deg*, group-wise comparisons at δ_0 were performed using the Mann–Whitney test as normal distribution was not assumed. We assessed longitudinal (i.e., time-related) differences between δ_0, $\delta_{ld1\text{-}5}$ and $\delta_{rl1\text{-}5}$ using the Kruskal Wallis test followed (for the serial T1ρ maps) or one-way ANOVA (for sample dimensions and pixel numbers). Correlations between $\Delta T1\rho(\delta_{ld1\text{-}5}, \delta_{rl1\text{-}5})$ and biomechanical and histological reference measures were quantified using Spearman's correlation coefficient ρ. Normally distributed data are

Table II
Histological, biomechanical, and T1ρ characteristics of human articular cartilage samples. Group-wise comparison of histologically intact (int) vs degenerative (deg) samples was performed using the Mann Whitney test for which the respective *p*-values are given. Significant differences are shown in **bold-type**. Data are given as mean ± standard deviation or median (interquartile ranges) as well as range. Of note, T1ρ values relate to the unloaded configuration (i.e., δ_0). Segmentation outlines included the entire cartilage sample (ECS) as well as the superficial (sf) and deep (dp) layer, respectively

		Mankin Sum Score	Tangent stiffness [MPa]	T1ρ [δ0] [ms]		
				ECS	sf	dp
all ($n = 42$)	M ± SD	4.5 ± 2.3	0.65 ± 0.55	91.7 (74.7–97.1)	96.7 (86.0–105.1)	85.1 (73.0–92.2)
	Range	0.0–11.0	0.01–2.56	40.8–130.0		
int ($n = 21$)	M ± SD	2.6 ± 1.1	0.97 ± 0.54	92.6 (75.0–100.4)	99.8 (86.3–117.1)	87.5 (68.8–95.3)
	Range	0.0–4.0	0.05–2.56	40.8–130.0		
deg ($n = 21$)	M ± SD	6.4 ± 1.5	0.33 ± 0.34	87.4 (74.7–94.2)	94.4 (86.0–103.9)	82.7 (74.3–91.6)
	Range	5.0–11.0	0.01–1.32	72.7–123.0		
***P*-value**		**< 0.001**	**< 0.001**	0.456	0.474	0.672

Table III
Absolute T1ρ values in response to consecutive loading ($\delta_{ld1\text{-}5}$) and unloading ($\delta_{rl1\text{-}5}$). Here, δ_0 refers to the absolute T1ρ values in the unloaded configuration, while $\delta_{ld[x]}$ and $\delta_{rl[x]}$ refer to the respective absolute T1ρ values in the loaded ($\delta_{ld[x]}$) and relaxed configurations ($\delta_{rl[x]}$) at time point x (of five serial measurements each under loading and relaxation conditions),). Data are given as median (interquartile range) [ms]. Segmentation included the entire cartilage sample (ECS) as well as superficial (sf) and deep (dp) layers. Kruskal–Wallis followed by Dunn's multiple comparison tests were used to detect longitudinal differences between δ_0, $\delta_{ld1\text{-}5}$ and $\delta_{rl1\text{-}5}$. Significant differences are displayed in **bold-type** and indicated by *p*-values. Also, details of the post-hoc tests following pair-wise comparisons are given in the last column. Abbreviations as in Table II

		δ0	δld1	δld2	δld3	δld4	δld5	δrl1	δrl2	δrl3	δrl4	δrl5	*p*-value	post-hoc test details
all (n = 42)	ECS	91.7 (74.7–97.1)	98.8 (89.3–114.5)	96.6 (82.7–110.4)	100.0 (91.3–120.0)	100.4 (88.8–109.3)	96.5 (87.3–106.0)	90.8 (82.8–102.8)	93.0 (84.9–101.7)	95.1 (86.7–103.2)	95.3 (85.4–107.4)	98.4 (86.2–105.9)	0.022	
	sf	96.7 (86.0–105.1)	99.4 (88.2–111.3)	100.1 (85.4–115.7)	98.2 (92.5–118.4)	96.4 (92.4–105.9)	94.6 (89.3–105.9)	100.5 (95.2–112.0)	104.5 (96.9–113.2)	105.7 (96.5–115.5)	104.2 (92.7–115.3)	106.1 (93.1–117.2)	0.137	
	dp	85.1 (73.0–92.2)	97.2 (86.1–109.4)	96.6 (80.9–107.1)	100.3 (87.7–118.5)	101.0 (84.3–108.9)	94.1 (84.3–107.6)	86.1 (77.8–99.0)	90.5 (79.6–102.0)	89.4 (81.0–98.1)	91.7 (79.4–101.0)	92.9 (79.0–103.5)	**<0.001**	δ_0 vs δ_{ld1}, δ_0 vs δ_{ld3}, δ_{ld3} vs δ_{rel1}
intact (n=21)	ECS	92.6 (75.0–100.4)	95.3 (81.4–112.6)	96.6 (81.8–109.4)	94.9 (90.4–114.0)	97.3 (87.8–108.6)	96.9 (86.8–107.2)	97.1 (81.8–108.5)	93.5 (87.2–109.5)	97.0 (85.7–110.2)	98.1 (83.8–107.6)	101.8 (87.5–106.9)	0.973	
	sf	99.8 (86.3–117.1)	98.0 (80.2–115.5)	100.6 (84.8–115.4)	95.7 (91.2–115.5)	97.9 (92.0–105.8)	96.7 (89.9–109.7)	107.3 (97.2–122.1)	105.4 (98.2–114.9)	109.9 (96.4–116.1)	105.1 (92.2–113.7)	112.8 (92.9–119.2)	0.592	
	dp	87.5 (68.8–95.3)	86.6 (82.4–112.5)	92.8 (75.5–106.0)	96.9 (85.4–112.8)	99.1 (83.0–107.2)	96.3 (83.4–106.4)	91.0 (75.5–101.2)	90.4 (79.0–107.7)	89.4 (76.7–105.1)	88.1 (80.0–102.4)	95.3 (77.7–105.8)	0.876	
degenerative (n=21)	ECS	87.4 (74.7–94.2)	103.8 (92.8–115.6)	97.7 (83.0–111.3)	111.4 (90.6–120.6)	100.6 (89.3–110.8)	94.5 (89.6–109.0)	90.3 (82.7–96.4)	92.2 (83.9–100.9)	93.7 (87.0–100.9)	93.6 (88.0–105.2)	93.9 (85.7–100.8)	**0.004**	δ_0 vs δ_{ld1}, δ_0 vs δ_{ld3}
	sf	94.4 (86.0–103.9)	102.6 (89.8–110.7)	97.6 (85.8–116.3)	103.7 (93.2–119.3)	96.3 (92.7–107.0)	94.4 (87.9–105.0)	98.9 (94.8–106.1)	101.8 (95.6–110.9)	103.8 (96.0–114.5)	99.7 (92.9–119.1)	104.8 (93.1–112.1)	0.411	
	dp	82.7 (74.3–91.6)	102.6 (94.8–110.9)	96.9 (83.0–108.7)	110.0 (89.2–119.9)	102.4 (84.7–112.6)	94.0 (86.3–115.4)	85.0 (77.7–91.2)	90.7 (79.7–101.0)	89.2 (81.0–94.8)	93.2 (78.6–100.3)	91.1 (79.0–101.2)	**<0.001**	δ_0 vs δ_{ld1}, δ_0 vs δ_{ld3}, δ_{ld1} vs δ_{rel1}, δ_{ld3} vs δ_{rel1}

given as mean ± standard deviation and non-normally distributed data as median (interquartile range). Level of significance was set to $P \leq 0.005$.

Results

General findings

All 42 samples underwent complete MR imaging and reference assessment. Histologically, samples displayed slight to moderate degenerative changes; the MSS distribution is given in Fig. 2(b). $N = 21$ samples each constituted the *int* and *deg* subgroup. All cartilage sample displayed signs of degeneration, i.e., no sample was graded as MSS 0. Analysis of the chondral samples revealed that no bone tissue was included. Significant differences between the *int* and *deg* subgroups were found for TS (0.97 ± 0.54 vs 0.33 ± 0.34 [MPa]; $P < 0.001$), while for T1ρ(δ_0), no significant degeneration-dependent differences were determined. In all samples, regardless of degeneration, T1ρ values tended to be higher in the superficial than deep layers. Mean sample height (as determined by micrometry) was 2.96 ± 0.38 mm in all samples. Additional histological, biomechanical and T1ρ(δ_0) characteristics are summarized in Table II.

Quantitative loading-induced changes

Quantitively, the chondral samples demonstrated changes in shape throughout the various loading conditions. First, mean sample height (−9.6 ± 23.8% [δ_{ld5} vs δ_0], −13.0 ± 23.5% [δ_{rl1} vs δ_0]; $P < 0.001$) and width (+7.4 ± 12.4% [δ_{ld5} vs δ_0], −3.3 ± 9.5% [δ_{rl1} vs δ_0]; $P < 0.001$) changed significantly. Mean pixel numbers decreased slightly, yet not significantly (116 ± 42 [δ_0], 114 ± 24 [δ_{ld5}] and 100 ± 35 [δ_{rl1}] [ECS]). Second, we found variable changes in T1ρ values (Table III). In *int* samples, mean T1ρ values were relatively consistent and not significantly different in response to loading. T1ρ slightly increased, primarily in the deep layer, while they remained grossly unaltered in the superficial layer. With unloading, the increases in T1ρ (as compared to δ_0) were persistent and primarily involved the superficial layer. In *deg* samples and in response to loading, T1ρ increased significantly and primarily in the deep layer ($P < 0.001$) and the entire sample ($P = 0.004$) as compared to δ_0; see Table III for post-hoc test details. More specifically, initially increased T1ρ gradually declined to δ_0 levels despite constantly upheld pressurization (in the superficial layer), while they were continuously elevated and undulating with largest changes noted at δ_{ld1} and δ_{ld3} (in the deep layer). With unloading, T1ρ values persistently increased (superficial layer) or gradually decreased to approach δ_0 values (deep layer).

Significant correlations were only found between TS and MSS ($\rho = -0.68$, $P < 0.001$). Consequently, we did not find significant correlations between TS or MSS and T1ρ(δ_0) or ΔT1ρ($\delta_{ld1\text{-}5}$, $\delta_{rl1\text{-}5}$).

Qualitative loading-induced changes

Qualitatively, T1ρ maps were largely reflective of these changes. We observed moderate increases in T1ρ with loading in *int* samples (Fig. 3) and discrepant responses to loading and unloading in *deg* samples. In some *deg* samples, these changes were inconsistent and undulating with variable increases and decreases in T1ρ despite constant pressurization. Focal signal hyperintensities were observed alongside more widespread signal alterations (Fig. 4). In other *deg* samples, loading-induced focal signal hyperintensities gradually increased and involved separate tissue areas (Fig. 5). With unloading, we found persistent

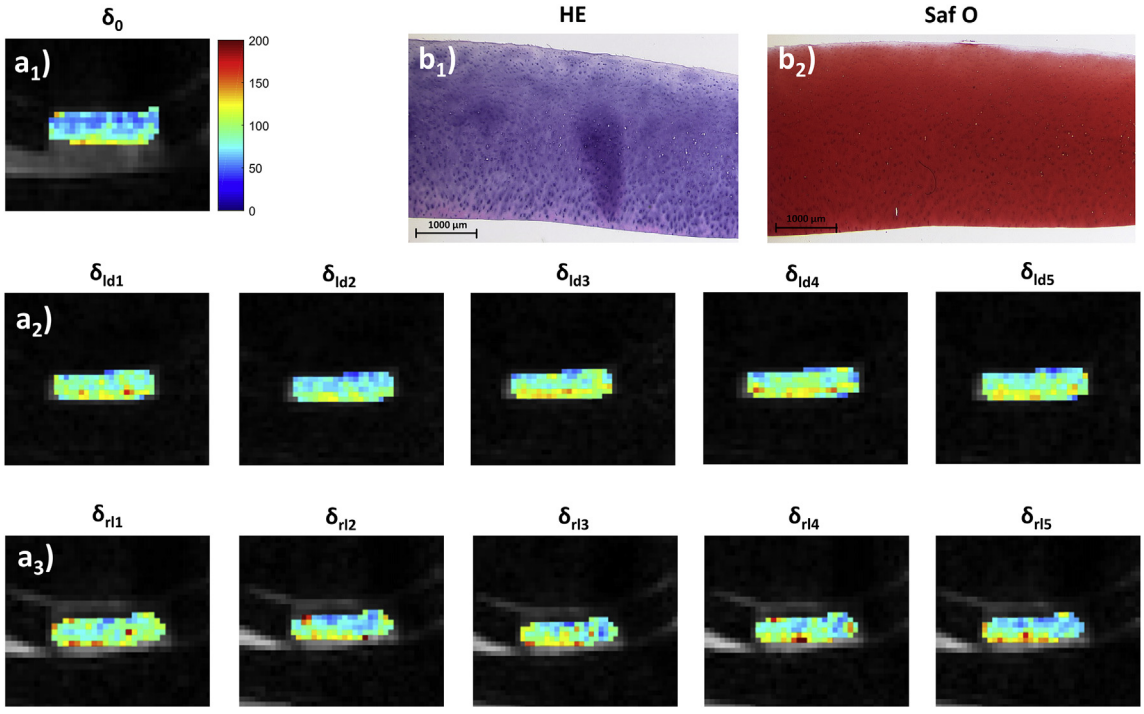

Fig. 3. Serial T1ρ maps (unloaded, δ_0 [a_1]) in response to sequential loading ($\delta_{ld1\text{-}5}$ [a_2]) and unloading ($\delta_{rl1\text{-}5}$ [a_3]) of histologically intact human articular cartilage. Loading-induced increases in T1ρ were moderate and extended throughout the entire tissue height to be persistent with unloading. Color-coded T1ρ maps were overlaid onto the corresponding morphological PDW image. Histologically, this sample displayed slight hypercellularity, but was otherwise normal, i.e., the surface was intact, proteoglycan staining intensity was normal and the tidemark intact (Mankin sum score 1). Hematoxylin and eosin (b_1) and Safranin O stainings (b_2). Note that sample surfaces are oriented downwards (in MR images, a) and upwards (in histological sections, b).

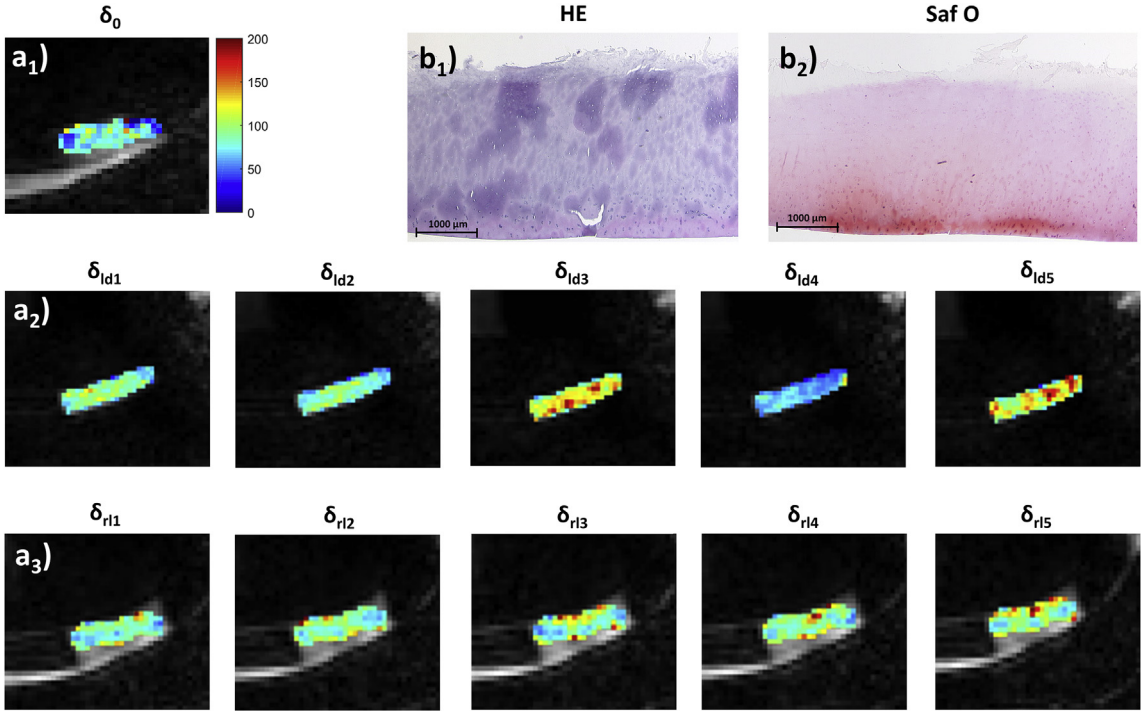

Fig. 4. Serial T1ρ maps of moderately degenerative human articular cartilage. Loading-induced changes in T1ρ ($\delta_{ld1} - \delta_{ld5}$) were inconsistent and disorganized with slight (δ_{ld1}, δ_{ld2}) and marked increases (δ_{ld3}, δ_{ld5}) observed alongside slight decreases (δ_{ld4}). With unloading, T1ρ values were persistently elevated and did not return to pre-loading levels (δ_0). Histologically, this sample displayed still moderate structural surface disintegration with clefts extending into the transitional zone, normal cellularity and moderately reduced proteoglycan staining intensity (Mankin sum score 5). Image order as in Fig. 3.

elevations in T1ρ beyond δ_0 levels in all samples, irrespective of degeneration (Figs. 3–5). Morphologically (as assessed on PDW images, not shown), we noted consistent loading-induced decreases in sample height, while signal intensity remained unaltered.

Discussion

The most important findings of our study are that variable changes in T1ρ were induced by sequential loading and unloading and that the response-to-loading and -unloading patterns were significantly different in *int* and *deg* cartilage.

Tissue functionality in intact tissue

Intact cartilage was characterized by consistent changes in T1ρ that were limited in extent and intensity. With loading, T1ρ values were increased, primarily in the deep layer, while after unloading, these were continuously elevated, primarily in the superficial layer. Several intra-tissue adaptive processes indicative of physiological load-bearing may be responsible. During loading, the radially oriented collagen fibres constituting the deep layer are spread out, which creates higher T1ρ signal intensity as a larger fraction of fibres is oriented at magic angle[26]. Moreover, condensation and deformation of the ECM induce interstitial water redistribution within and out of the tissue and increases in proteoglycan and collagen concentration[27]. As T1ρ is only weakly (if at all) associated with the individual tissue constituents[11,12,28], it is the slow spin-motions and their interactions with the fluid and solid phases[29] that are the likely imaging correlates of the loading-induced increases in T1ρ. However, the exact sensitivity and specificity of T1ρ remains to be clarified with some studies suggesting specificity for proteoglycans[28,30], while others refuted any such specificity[11,12]. Nonetheless, it is commonly agreed that T1ρ is a surrogate parameter for the tissue's macromolecular constitution and functional properties[5,7,8,13,14].

Tissue functionality in degenerative tissue

In contrast, *deg* samples were characterized by marked, yet inconsistent loading-induced changes in T1ρ. We found disparate layer-wise responses with moderate, yet non-significant increases in the superficial layer and stronger, partially significant increases in the deep layer. Remarkably, T1ρ values displayed undulating longitudinal changes despite constant pressurization which may be due to degeneration-related changes in tissue structure and composition. With increasing (histological) degeneration, the tissue softens considerably, which is confirmed in our study, and the fractions of the cartilage constituents are altered. Early cartilage degeneration is characterized by a loss in proteoglycans and fixed-charge density alongside collagen fibre disorganization, while collagen and water contents remain unaltered. Thereby, local tissue strains are increased when the tissue is loaded[31]. More advanced degeneration is defined by marked compositional and structural changes and decreased ability to withstand loading, which accelerates tissue degeneration and brings about its eventual disintegration, failure and loss[32]. When intact cartilage is loaded, its viscoelasticity shields the ECM from excessive stresses by efficient fluid pressurization and energy dissipation[33]. Supposedly, these physiological mechanisms provide the imaging correlates of our study, i.e., the consistent changes in T1ρ. However, when degenerative cartilage is loaded, its altered structure and composition compromise intrinsic stiffness and increase compliance, while permeability and flow-dependent behaviours are affected to a lesser extent[33,34].

The significant loading-induced increases in T1ρ of *deg* samples are reflective of these phenomena. The undulating changes in T1ρ are indicative of extended and incoherent adaptive intra-tissue

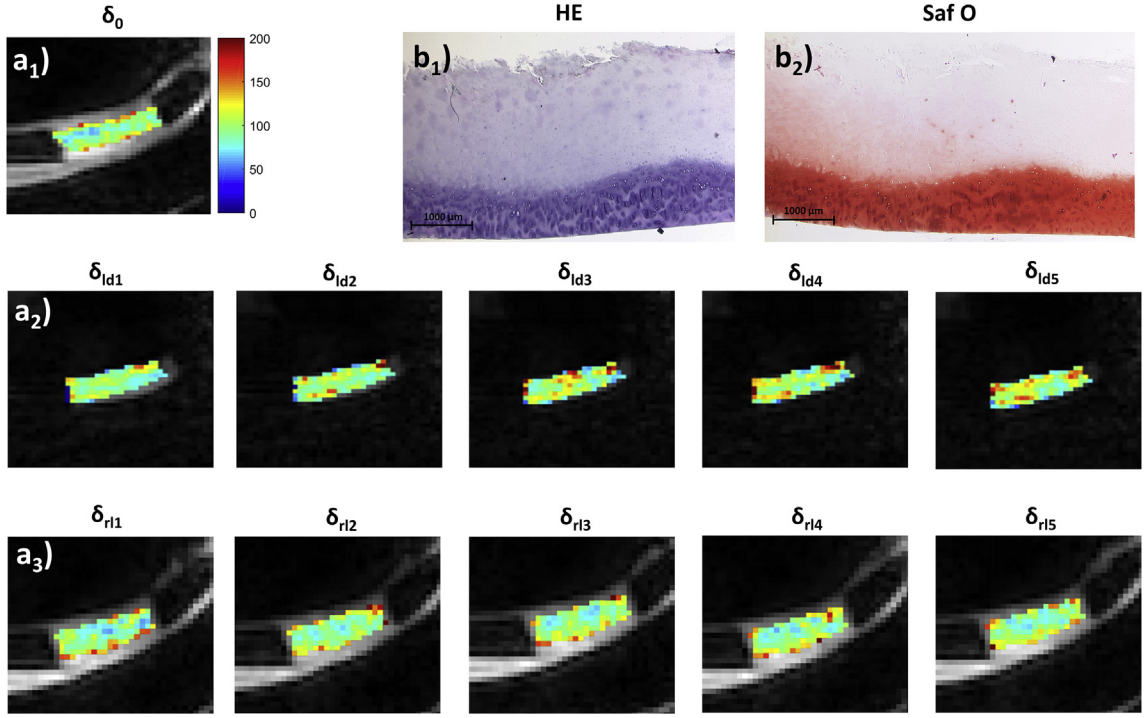

Fig. 5. Serial T1ρ maps of moderately degenerative human articular cartilage. Increases in T1ρ were gradually increasing under constant sample pressurization. The increases were persistent beyond δ_0 levels under relaxation. Histologically, this sample also displayed still moderate structural surface disintegration (with clefts extending into the transitional zone), diffuse hypercellularity (not shown at this magnification) and moderately reduced proteoglycan staining intensity (Mankin sum score 7). Image order as in Fig. 3.

processes prior to equilibration. Our study indicates that serial T1ρ maps as a function of time (and loading) are a promising method to visualize the tissue's load-bearing capacities and may provide more relevant information than mere quantitative changes. However, both T1ρ(δ_0) and ΔT1ρ were characterized by substantial standard deviation, which limits their diagnostic acuity. Another aspect pertains to the relation of statistical significance and scientific and/or diagnostic relevance. In biomedical research, statistical significance does not necessarily translate to scientific or even diagnostic relevance and, correspondingly, neither does statistical non-significance translate to the absence of relevance. Despite the implementation of a stringent threshold of $P < 0.005$ and the presence of substantial standard deviations, statistically significant differences in T1ρ indicative of inconsistent and disorganized load bearing were found in degenerative samples and in response to loading. In diagnostic contexts, these findings are not likely to be present in every cartilage sample, joint area, or patient studied by serial T1ρ mapping; however, wherever present, such inconsistent longitudinal changes are indicative of aberrant tissue functionality and a sign of (histological) degeneration.

We observed similar changes in T1ρ during relaxation in all samples, regardless of degeneration. While loading-induced increases in T1ρ subsided with unloading, they did not completely recover δ_0 values, at least within the provided imaging time. Persistent increases in T1ρ during relaxation primarily involved the superficial layer, which is plausible as it is softest and undergoes largest deformation (during loading[35]) and consecutive recovery processes (during relaxation).

Previous studies focusing on loading-induced changes in T1ρ reported inconsistent (and partially contradictory) results, i.e., increases[8,36] and decreases[7,13]. These discrepancies are most likely due to differences in species, study designs, loading and imaging protocols and segmentation techniques. The finding of larger mean changes in T1ρ in degenerative cartilage is in line with earlier studies[5,6].

No significant correlations were found between the histological and biomechanical reference measures and T1ρ(δ_0) or ΔT1ρ. This is not surprising as T1ρ is a measure of cartilage composition (rather than structure), and the tissue's biomechanical properties are related more to matrix integrity than to matrix composition[37].

Limitations

Technically, our loading device allows standardized and reproducible loading in a more physiological configuration than previous devices[8,14,15,38,39]. Yet, this setup is not truly physiological as it allows only uni-axial compression along the mechanical leg axis. Similarly, the stabilizing structures in and around the joint are not considered. Biomechanically, loading therefore equalled conformed and confined compression creep tests of compliant, yet incompressible cartilage samples of variable degeneration constrained by the underlying artificial bone. Wirosil® (the artificial cartilage-mimicking layer) is less stiff than human cartilage[15], thereby allowing for compression and shearing, which is more reflective of *in vivo* weight-bearing than compression or shearing alone[40]. We cut cartilage samples to standard size (8 mm) and height (3 mm) above the subchondral lamella. This approach may have introduced inaccuracy as height at the medial femur is variable[41]. Consequently, even slight differences in including the deep cartilage region may be relevant because of its secondary role in tissue pressurization[42]. Yet, the superficial zone is most relevant in retaining tissue pressurization[43] and was left unaltered. On average, 7–8 pixels constituted the entire sample height. Therefore, we chose a conservative manual segmentation approach to reduce partial volume artifacts. This approach, however, increases the risk of disregarding superficial tissue areas in the unloaded reference images (and, consequently, T1ρ(δ_0) quantification) that may secondarily be pushed into the segmentation outlines.

Biologically, samples were obtained from total knee replacements, which explains why seemingly intact samples showed signs of early degeneration, too. OA as a whole-joint disease causes changes to all cartilaginous tissues in a joint, even in joint areas not primarily affected. Consequently, macroscopically intact tissue from an osteoarthritic joint is not the same as macroscopically intact tissue from a healthy joint. Our study therefore defines cartilage functionality of grossly intact cartilage with minor signs of degeneration. Alternative sample sources such as organ donor networks, tumor endoprosthesis and major amputations should be included to be more reflective of the entire spectrum of health and disease. Moreover, histological/histochemical methods may not provide the ideal reference measure to distinguish intact from degenerative cartilage. The Mankin classification[24] and the more recently introduced OARSI scores[44,45] are closely related and provide excellent tools for histological scoring of cartilage quality. Yet, these methods likely fail to indicate compositional and ultrastructural tissue properties that determine cartilage functionality and its imaging correlates. Accordingly, future studies should include more sophisticated referencing techniques such as microspectroscopy or polarized light microscopy[46].

Additionally, more physiological setups integrating human cadaver joints are necessary to confirm our findings before the *in vivo* translation should be undertaken. Several factors, e.g., storage and measurement conditions, affect tissue properties and may be responsible for potential differences between *in vivo* and *in vitro* studies. We performed measurements at room temperature (and not at body temperature) with the consequence of possibly differing T1ρ relaxation times. As relaxation characteristics and temperature are linearly dependent[47], statistical relations are likely maintained *in vivo*. Moreover, to include the pneumatic mechanism the experimental setup used a single-channel coil located at the medial compartment. As clinical workflows commonly use dedicated multi-channel knee coils, further standardization and validation work is necessary.

Conclusions

In conclusion, cartilage mechanosensitivity is related to histological degeneration and assessable by serial T1ρ mapping. Unloaded, T1ρ characteristics are similar in intact and degenerative cartilage, yet their response-to-loading patterns are different. In intact cartilage, T1ρ values are altered consistently, which is indicative of organized load-bearing. In degenerative cartilage, T1ρ values are undulating, which is indicative of disorganized load-bearing. Serial T1ρ mapping can therefore be considered a surrogate parameter of tissue functionality and may provide an exciting scientific framework to further differentiate cartilage in health and disease. Nonetheless, in this era of much sought-after reproducibility of research, future translational studies are necessary to confirm that the statistically significant differences observed in this study are of scientific and diagnostic relevance. Accordingly, the deep layer of cartilage should be considered the diagnostically relevant structure to differentiate the tissue's functional status.

Author contributions

Study conception and design: SN, DT.
Acquisition of data: SN, MP, CS, JT, DT.
Analysis and interpretation of data: SN, MT, MK, CK, DT.
Drafting of the article: SN, LH, CK, DT.
Provision of study materials: MK, MT

Statistical expertise: SN, DT

Obtaining of funding: SN, DT

Administrative, technical, or logistic support: LH, MK, DS, CS, MT, CK

Critical revision of the article for important intellectual content: all authors.

Final approval of the version to be submitted: all authors.

Guarantors of integrity of entire study: SN (snebelung@ukaachen.de), DT (dtruhn@ukaachen.de).

Conflict of interest statement

The authors do not have any financial, consulting or personal relationships with other people or organizations to disclose.

Role of the funding source

This research project was supported by the START Program of the Faculty of Medicine, RWTH Aachen, Germany granted to SN (691702) and through the START rotation programme granted to DT. The sponsor had no role in the study design; in the collection, analysis and interpretation of data; in the writing of the report; and in the decision to submit the manuscript for publication.

Acknowledgements

This research project was supported by grants from the Deutsche Forschungsgemeinschaft (NE 2136/3-1) and the START Program of the Faculty of Medicine, RWTH Aachen, Germany, through means of a grant (SN, 691702) and the START rotation programme (D.T.). We gratefully acknowledge Philips Healthcare for providing the T1ρ sequence.

Supplementary data

Supplementary data to this article can be found online at https://doi.org/10.1016/j.joca.2019.07.006.

References

1. Vincent TL, Wann AKT. Mechanoadaptation: articular cartilage through thick and thin. J Physiol 2019 Mar;597(5):1271–81, https://doi.org/10.1113/JP275451. Epub 2018 Jul 29.
2. Loeser RF, Goldring SR, Scanzello CR, Goldring MB. Osteoarthritis: a disease of the joint as an organ. Arthritis Rheum 2012;64:1697–707.
3. Bader DL, Salter DM, Chowdhury TT. Biomechanical influence of cartilage homeostasis in health and disease. Arthritis 2011;2011:979032.
4. Haapala J, Arokoski J, Pirttimaki J, Lyyra T, Jurvelin J, Tammi M, *et al.* Incomplete restoration of immobilization induced softening of young beagle knee articular cartilage after 50-week remobilization. Int J Sports Med 2000;21:76–81.
5. Souza RB, Kumar D, Calixto N, Singh J, Schooler J, Subburaj K, *et al.* Response of knee cartilage T1rho and T2 relaxation times to in vivo mechanical loading in individuals with and without knee osteoarthritis. Osteoarthr Cartil 2014;22:1367–76.
6. Subburaj K, Souza RB, Stehling C, Wyman BT, Le Graverand-Gastineau MP, Link TM, *et al.* Association of MR relaxation and cartilage deformation in knee osteoarthritis. J Orthop Res 2012;30:919–26.
7. Souza RB, Stehling C, Wyman BT, Hellio Le Graverand MP, Li X, Link TM, *et al.* The effects of acute loading on T1rho and T2 relaxation times of tibiofemoral articular cartilage. Osteoarthr Cartil 2010;18:1557–63.
8. Nebelung S, Sondern B, Oehrl S, Tingart M, Rath B, Pufe T, *et al.* Functional MR imaging mapping of human articular cartilage response to loading. Radiology 2017;282:464–74.
9. MacKay JW, Low SBL, Smith TO, Toms AP, McCaskie AW, Gilbert FJ. Systematic review and meta-analysis of the reliability and discriminative validity of cartilage compositional MRI in knee osteoarthritis. Osteoarthr Cartil 2018;26:1140–52.
10. Palmer AJ, Brown CP, McNally EG, Price AJ, Tracey I, Jezzard P, *et al.* Non-invasive imaging of cartilage in early osteoarthritis. Bone Joint Lett J 2013;95-B:738–46.
11. Thuring J, Linka K, Itskov M, Knobe M, Hitpass L, Kuhl C, *et al.* Multiparametric MRI and computational modelling in the assessment of human articular cartilage properties: a comprehensive approach. BioMed Res Int 2018;2018:9460456.
12. van Tiel J, Kotek G, Reijman M, Bos PK, Bron EE, Klein S, *et al.* Is T1rho mapping an alternative to delayed gadolinium-enhanced MR imaging of cartilage in the assessment of sulphated glycosaminoglycan content in human osteoarthritic knees? An in vivo validation study. Radiology 2016;279:523–31.
13. Hamada H, Nishii T, Tamura S, Tanaka H, Wakayama T, Sugano N. Comparison of load responsiveness of cartilage T1rho and T2 in porcine knee joints: an experimental loading MRI study. Osteoarthr Cartil 2015;23:1776–9.
14. Nebelung S, Sondern B, Jahr H, Tingart M, Knobe M, Thuring J, *et al.* Non-invasive T1rho mapping of the human cartilage response to loading and unloading. Osteoarthr Cartil 2018;26:236–44.
15. Nebelung S, Post M, Raith S, Fischer H, Knobe M, Braun B, *et al.* Functional in situ assessment of human articular cartilage using MRI: a whole-knee joint loading device. Biomech Model Mechanobiol 2017;16:1971–86.
16. Nebelung S, Brill N, Tingart M, Pufe T, Kuhl C, Jahr H, *et al.* Quantitative OCT and MRI biomarkers for the differentiation of cartilage degeneration. Skelet Radiol 2016;45:505–16.
17. Kellgren JH, Lawrence JS. Radiological assessment of osteo-arthrosis. Ann Rheum Dis 1957;16:494–502.
18. Terukina M, Fujioka H, Yoshiya S, Kurosaka M, Makino T, Matsui N, *et al.* Analysis of the thickness and curvature of articular cartilage of the femoral condyle. Arthroscopy 2003;19:969–73.
19. Mainil-Varlet P, Aigner T, Brittberg M, Bullough P, Hollander A, Hunziker E, *et al.* Histological assessment of cartilage repair: a report by the histology endpoint committee of the international cartilage repair society (ICRS). J Bone Joint Surg Am 2003;85-A(Suppl 2):45–57.
20. Nebelung S, Post M, Knobe M, Tingart M, Emans P, Thüring J, *et al.* Detection of early-stage degeneration in human articular cartilage by multiparametric MR imaging mapping of tissue functionality. Sci Rep 2019;9:5895.
21. Walpole SC, Prieto-Merino D, Edwards P, Cleland J, Stevens G, Roberts I. The weight of nations: an estimation of adult human biomass. BMC Public Health 2012;12:439.
22. Li LP, Herzog W. Strain-rate dependence of cartilage stiffness in unconfined compression: the role of fibril reinforcement versus tissue volume change in fluid pressurization. J Biomech 2004;37:375–82.
23. Jurvelin JS, Buschmann MD, Hunziker EB. Optical and mechanical determination of Poisson's ratio of adult bovine humeral articular cartilage. J Biomech 1997;30:235–41.
24. Mankin HJ, Dorfman H, Lippiello L, Zarins A. Biochemical and metabolic abnormalities in articular cartilage from osteo-

arthritic human hips. II. Correlation of morphology with biochemical and metabolic data. J Bone Joint Surg Am 1971;53:523–37.
25. Gahunia HK, Babyn P, Lemaire C, Kessler MJ, Pritzker KP. Osteoarthritis staging: comparison between magnetic resonance imaging, gross pathology and histopathology in the rhesus macaque. Osteoarthr Cartil 1995;3:169–80.
26. Grunder W. MRI assessment of cartilage ultrastructure. NMR Biomed 2006;19:855–76.
27. Grunder W, Kanowski M, Wagner M, Werner A. Visualization of pressure distribution within loaded joint cartilage by application of angle-sensitive NMR microscopy. Magn Reson Med 2000;43:884–91.
28. Wong CS, Yan CH, Gong NJ, Li T, Chan Q, Chu YC. Imaging biomarker with T1rho and T2 mappings in osteoarthritis - in vivo human articular cartilage study. Eur J Radiol 2013;82:647–50.
29. Wang L, Regatte RR. T1rho MRI of human musculoskeletal system. J Magn Reson Imaging 2015;41:586–600.
30. Oei EH, van Tiel J, Robinson WH, Gold GE. Quantitative radiologic imaging techniques for articular cartilage composition: toward early diagnosis and development of disease-modifying therapeutics for osteoarthritis. Arthritis Care Res 2014;66:1129–41.
31. Saarakkala S, Julkunen P, Kiviranta P, Makitalo J, Jurvelin JS, Korhonen RK. Depth-wise progression of osteoarthritis in human articular cartilage: investigation of composition, structure and biomechanics. Osteoarthr Cartil 2010;18:73–81.
32. Rahmati M, Nalesso G, Mobasheri A, Mozafari M. Aging and osteoarthritis: central role of the extracellular matrix. Ageing Res Rev 2017;40:20–30.
33. Setton LA, Elliott DM, Mow VC. Altered mechanics of cartilage with osteoarthritis: human osteoarthritis and an experimental model of joint degeneration. Osteoarthr Cartil 1999;7:2–14.
34. Kumar R, Pierce DM, Isaksen V, Davies CL, Drogset JO, Lilledahl MB. Comparison of compressive stress-relaxation behavior in osteoarthritic (ICRS graded) human articular cartilage. Int J Mol Sci 2018;19.
35. Chen SS, Falcovitz YH, Schneiderman R, Maroudas A, Sah RL. Depth-dependent compressive properties of normal aged human femoral head articular cartilage: relationship to fixed charge density. Osteoarthr Cartil 2001;9:561–9.
36. Nebelung S, Sondern B, Jahr H, Tingart M, Knobe M, Thüring J, *et al.* Non-invasive T1ρ Mapping of the Human Cartilage Response to Loading and Unloading. Osteoarthritis and cartilage; 2017.
37. Franz T, Hasler EM, Hagg R, Weiler C, Jakob RP, Mainil-Varlet P. In situ compressive stiffness, biochemical composition, and structural integrity of articular cartilage of the human knee joint. Osteoarthr Cartil 2001;9:582–92.
38. Nebelung S, Brill N, Muller F, Tingart M, Pufe T, Merhof D, *et al.* Towards Optical Coherence Tomography-based elastographic evaluation of human cartilage. J Mech Behav Biomed Mater 2016;56:106–19.
39. Juras V, Bittsansky M, Majdisova Z, Szomolanyi P, Sulzbacher I, Gabler S, *et al.* In vitro determination of biomechanical properties of human articular cartilage in osteoarthritis using multi-parametric MRI. J Magn Reson 2009;197:40–7.
40. Chan DD, Cai L, Butz KD, Trippel SB, Nauman EA, Neu CP. In vivo articular cartilage deformation: noninvasive quantification of intratissue strain during joint contact in the human knee. Sci Rep 2016;6:19220.
41. Frisbie DD, Cross MW, McIlwraith CW. A comparative study of articular cartilage thickness in the stifle of animal species used in human pre-clinical studies compared to articular cartilage thickness in the human knee. Vet Comp Orthop Traumatol 2006;19:142–6.
42. Wong M, Carter DR. Articular cartilage functional histomorphology and mechanobiology: a research perspective. Bone 2003;33:1–13.
43. Krishnan R, Park S, Eckstein F, Ateshian GA. Inhomogeneous cartilage properties enhance superficial interstitial fluid support and frictional properties, but do not provide a homogeneous state of stress. J Biomech Eng 2003;125:569–77.
44. Custers RJ, Creemers LB, Verbout AJ, van Rijen MH, Dhert WJ, Saris DB. Reliability, reproducibility and variability of the traditional histologic/histochemical grading system vs the new OARSI osteoarthritis cartilage histopathology assessment system. Osteoarthr Cartil 2007;15:1241–8.
45. Pearson RG, Kurien T, Shu KS, Scammell BE. Histopathology grading systems for characterisation of human knee osteoarthritis–reproducibility, variability, reliability, correlation, and validity. Osteoarthr Cartil 2011;19:324–31.
46. Oinas J, Rieppo L, Finnila MA, Valkealahti M, Lehenkari P, Saarakkala S. Imaging of osteoarthritic human articular cartilage using fourier transform infrared microspectroscopy combined with multivariate and univariate analysis. Sci Rep 2016;6:30008.
47. Bottomley PA, Foster TH, Argersinger RE, Pfeifer LM. A review of normal tissue hydrogen NMR relaxation times and relaxation mechanisms from 1-100 MHz: dependence on tissue type, NMR frequency, temperature, species, excision, and age. Med Phys 1984;11:425–48.